

# PPAR- $\gamma$ is a major driver of the accumulation and phenotype of adipose tissue T<sub>reg</sub> cells

Daniela Cipolletta<sup>1</sup>, Markus Feuerer<sup>1†</sup>, Amy Li<sup>1</sup>, Nozomu Kamei<sup>2†</sup>, Jongsoo Lee<sup>2</sup>, Steven E. Shoelson<sup>2</sup>, Christophe Benoist<sup>1</sup> & Diane Mathis<sup>1</sup>

Obesity and type-2 diabetes have increased markedly over the past few decades, in parallel. One of the major links between these two disorders is chronic, low-grade inflammation<sup>1</sup>. Prolonged nutrient excess promotes the accumulation and activation of leukocytes in visceral adipose tissue (VAT) and ultimately other tissues, leading to metabolic abnormalities such as insulin resistance, type-2 diabetes and fatty-liver disease. Although invasion of VAT by pro-inflammatory macrophages is considered to be a key event driving adipose-tissue inflammation and insulin resistance, little is known about the roles of other immune system cell types in these processes. A unique population of VAT-resident regulatory T (T<sub>reg</sub>) cells was recently implicated in control of the inflammatory state of adipose tissue and, thereby, insulin sensitivity<sup>2</sup>. Here we identify peroxisome proliferator-activated receptor (PPAR)- $\gamma$ , the 'master regulator' of adipocyte differentiation, as a crucial molecular orchestrator of VAT T<sub>reg</sub> cell accumulation, phenotype and function. Unexpectedly, PPAR- $\gamma$  expression by VAT T<sub>reg</sub> cells was necessary for complete restoration of insulin sensitivity in obese mice by the thiazolidinedione drug pioglitazone. These findings suggest a previously unknown cellular mechanism for this important class of thiazolidinedione drugs, and provide proof-of-principle that discrete populations of T<sub>reg</sub> cells with unique functions can be precisely targeted to therapeutic ends.

A unique population of Foxp3<sup>+</sup> CD4<sup>+</sup> T<sub>reg</sub> cells was recently found in the VAT of normal individuals<sup>2</sup>, at a much higher fraction of the CD4<sup>+</sup> T-cell compartment than that usually observed in lymphoid or other non-lymphoid tissues. VAT T<sub>reg</sub> cells had a readily distinguishable phenotype from that of their counterparts in the spleen and lymph nodes, including a distinct gene expression profile, T-cell receptor repertoire, and pattern of chemokine and chemokine receptor expression. Adipose tissue inflammation and both local and systemic

metabolic indices were improved or worsened by global enrichment or impoverishment, respectively, of T<sub>reg</sub> cells<sup>2-4</sup>. However, a lack of appropriate reagents has so far precluded an assessment of the precise role of fat-resident T<sub>reg</sub> cells.

The molecules that orchestrate the distinctive properties of VAT T<sub>reg</sub> cells are unknown. Comparing the gene expression profiles of mouse visceral fat and lymphoid organ T<sub>reg</sub> cells, we were struck by the increased level of transcripts encoding the nuclear receptor PPAR- $\gamma$  in the former (Fig. 1a and Supplementary Fig. 1a). The specificity of this increase was highlighted by a comparison of *Pparg* transcript levels across a large library of microarray data sets (more than 350) encompassing T cells of diverse subsets, activation statuses and localizations (Fig. 1b). Because of the crucial role of PPAR- $\gamma$  in adipocyte differentiation, as well as its anti-inflammatory activities<sup>5</sup>, we speculated that its expression in VAT T<sub>reg</sub> cells might be responsible for at least some of their unique features.

To identify genes that were positively or negatively correlated with *Pparg* expression, we performed a clustering analysis across transcript profiles obtained from VAT and lymph node T<sub>reg</sub> cells of mice differing in their metabolic state: either lean (C57Bl/6 (B6) animals of various ages kept on normal chow) or obese (B6.*Lep*<sup>ob/ob</sup> (ob/ob) animals of varying age on normal chow or B6 animals on a high-fat diet (HFD)) (Supplementary Fig. 1b, c). The set of loci whose expression was co- or anti-correlated with *Pparg* transcript levels encompassed the majority of those most strongly up- (red) or down- (blue) regulated, respectively, in visceral fat versus lymphoid tissue T<sub>reg</sub> cells<sup>2</sup> (Fig. 1c). The co-clustered transcripts included many that encode chemokines or chemokine receptors involved in leukocyte migration and extravasation (for example, *Ccr1*, *Ccr3*, *Cxcr6*, *Cxcl2* and *Cxcl3*), several encoding molecules involved in lipid metabolism (*Pcyt1a* and *Dgat1*), and *Il10* transcripts.

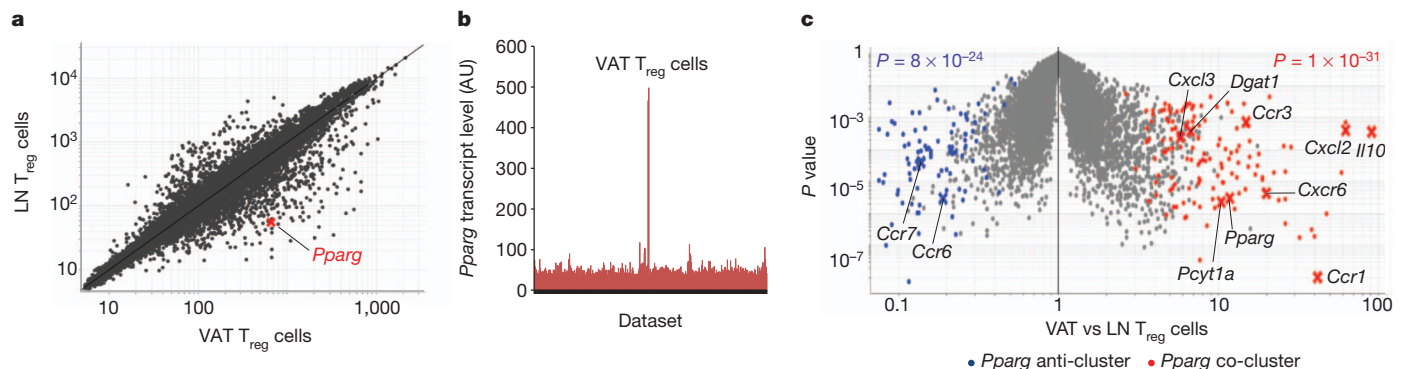


**Figure 1** | Transcripts directly or inversely correlated with *Pparg* expression in VAT T<sub>reg</sub> cells. **a**, Microarray analysis. Normalized expression values for transcripts isolated from T<sub>reg</sub> cells from epididymal fat versus lymph node (LN) of 30-week-old retired-breeder B6 males (in triplicate). **b**, Expression of *Pparg* in a library of microarray data sets from diverse T-cell populations: different

subsets, activation statuses or locations. AU, arbitrary units. **c**, A volcano plot comparing gene expression in VAT and lymph node T<sub>reg</sub> cells of normal-chow fed B6 mice. The *Pparg* co- and anti-cluster transcripts defined in Supplementary Fig. 1b are superimposed in red and blue, respectively. Some of the characteristic VAT T<sub>reg</sub> genes are indicated. *P* values are from a chi-squared test.

<sup>1</sup>Division of Immunology, Department of Microbiology and Immunobiology, Harvard Medical School, Boston, Massachusetts 02115, USA. <sup>2</sup>Joslin Diabetes Center and Department of Medicine, Harvard Medical School, Boston, Massachusetts 02215, USA. †Present addresses: German Cancer Research Center (DKFZ), 69120 Heidelberg, Germany (M.F.); The University of Tokyo, Tokyo 113-8655, Japan (N.K.).

We directly evaluated the role of PPAR- $\gamma$  in specifying the VAT T<sub>reg</sub> cell phenotype by retrovirally transducing *Foxp3* alone or together with *Pparg* into naive CD4<sup>+</sup> T cells activated *in vitro* with anti-CD3/CD28-coated beads (neither transcription factor being expressed at detectable levels in the host CD4<sup>+</sup> T cells). Two isoforms of PPAR- $\gamma$  have been described, referred to as PPAR- $\gamma$ 1 and PPAR- $\gamma$ 2 (ref. 5); although adipocytes are known to express both of them, the isoform(s) made by T lymphocytes is not well characterized. Feature-level analysis of *Pparg* transcripts, exploiting our existing Affymetrix ST 1.0 microarray data, showed that messenger RNAs corresponding to both PPAR- $\gamma$ 1 and PPAR- $\gamma$ 2 were expressed by VAT T<sub>reg</sub> cells, with predominance of the former (Supplementary Fig. 2a), whereas the low-level transcripts made by the other T-cell populations primarily encoded PPAR- $\gamma$ 2 (not shown). Therefore, we evaluated the ability of each isoform to cooperate with *Foxp3* to promote the VAT T<sub>reg</sub> cell gene expression signature. Most transcripts are distributed in a grey cloud along the diagonal in the fold-change/fold-change (FC/FC) plot of Fig. 2a, showing that *Pparg1* and *Pparg2* induced the expression of a similar set of genes when co-transduced with *Foxp3*; the slight tilt towards the *x*-axis indicates that *Pparg1* transduction was slightly more potent. Each isoform promoted expression of the above-discussed *Pparg* co-cluster (red cloud along the diagonal), although only *Pparg1* repressed expression of the bulk of the *Pparg* anti-cluster (blue cloud along the *x*-axis). Similarly, as illustrated most clearly by the *Pparg* plus *Foxp3* versus *Foxp3* alone 'volcano plots' (Fig. 2b, c), each PPAR- $\gamma$  isoform could collaborate with *Foxp3* to upregulate a substantial fraction of the genes characteristic of the VAT T<sub>reg</sub> cell up-signature (pink, skewed to the right in Fig. 2b, c). However, the corresponding down-signature was partially recapitulated only after *Pparg1* plus *Foxp3* transduction (green, skewed to the left in Fig. 2c but not in Fig. 2d).

Because adequate PPAR- $\gamma$  ligand might not be available in this *in vitro* context, we explored the effect of adding a synthetic agonist, the thiazolidinedione (TZD) drug pioglitazone (Pio). Twenty-four hours after retroviral infection, double (*Pparg1* plus *Foxp3*, or *Pparg2* plus *Foxp3*) or single (*Foxp3* alone) transductants were treated with Pio for 48 h. The most notable effect of this agonist, whether in the context of *Pparg1* or *Pparg2*, was the augmentation of a set of 'lipid metabolism' genes, some of which were reported to be differentially expressed in VAT versus lymph node T<sub>reg</sub> cells in a previous *ex vivo* microarray analysis<sup>2</sup>. This influence was most obvious on FC/FC plots (Fig. 2d, e), which isolate the effect of Pio in the context of each isoform (as aligned towards the *x*-axis). Upregulated genes involved in lipid metabolism included those coding for fatty-acid transporters (*Cd36* and *Slc27a2*), enzymes involved in fatty-acid synthesis (*Lipe* and *Scd1*), an enzyme essential for fatty-acid oxidation (*Cpt1a*), an enzyme responsible for the synthesis of triglycerides (*Dgat1*), and a lipid-droplet-associated protein (*Plin2*). Similar results were obtained with rosiglitazone, another TZD drug, or with GW1929, a potent non-TZD PPAR- $\gamma$  agonist (Supplementary Fig. 2b, c; note change in axis labels compared with Fig. 2d, e). The fact that PPAR- $\gamma$  could cooperate with *Foxp3* to impose a VAT T<sub>reg</sub> cell phenotype on naive CD4<sup>+</sup> T cells raised the question of whether the two transcription factors interact in some way. Indeed, both PPAR- $\gamma$  isoforms were co-immunoprecipitated with *Foxp3* in transduced HEK293 cells, arguing that they have the potential to interact, either directly or within a shared complex (Fig. 2f). (Unfortunately, we could not obtain adequate material from *ex vivo* T cells to perform an analogous experiment.)

To assess the importance of PPAR- $\gamma$  for the VAT T<sub>reg</sub> phenotype *in vivo*, we abrogated its expression specifically in T<sub>reg</sub> cells by crossing a mouse line carrying 'floxed' *Pparg* with a line expressing the Cre recombinase under the dictates of *Foxp3* promoter/enhancer elements. The T<sub>reg</sub> cell specificity of Cre expression in such mice has been validated in several contexts. At 25 weeks, the resulting mutants had lower fractions and numbers of VAT T<sub>reg</sub> cells than their *Pparg* wild-type littermates (carrying the *Foxp3-Cre* transgene); by contrast, the

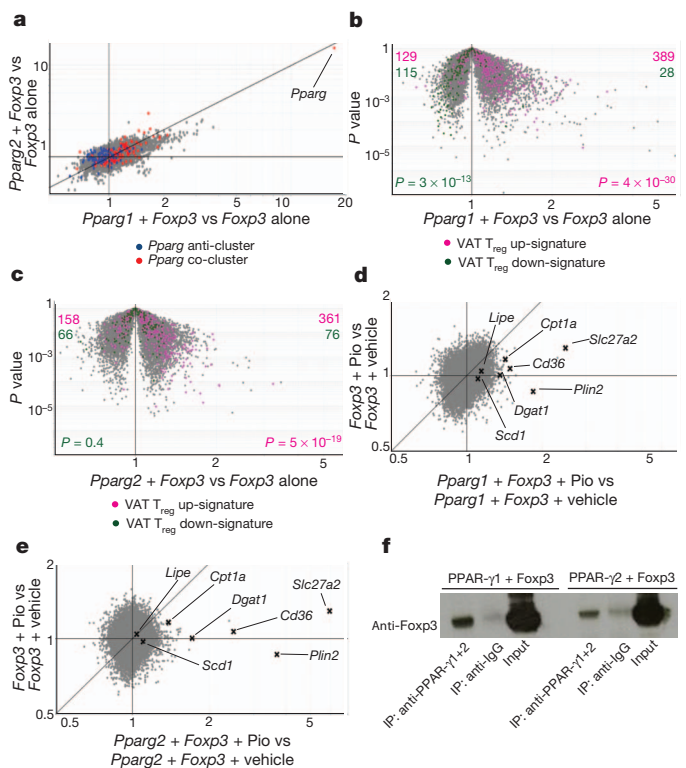


**Figure 2 | Cooperation between PPAR- $\gamma$  and Foxp3.** Naive CD4<sup>+</sup> CD25<sup>-</sup> T cells were stimulated *ex vivo* and transduced with retroviruses encoding *Foxp3* (MSCV IRES-GFP) plus *Pparg1* or *Pparg2* (both MSCV IRES-Thy1.1). Cells were sorted for green fluorescent protein (GFP) and/or Thy1.1 positivity before RNA processing. **a**, An FC/FC plot comparing gene expression values for double transductants (*Pparg1* plus *Foxp3*) versus single transductants (*Foxp3* alone) (*x*-axis), and parallel double transductants (*Pparg2* plus *Foxp3*) versus single transductants (*Foxp3* alone) (*y*-axis). *Pparg* co- and anti-cluster genes are superimposed in red and blue, respectively. **b**, **c**, Genes from the VAT T<sub>reg</sub> cell up- and down-signature highlighted in pink and green, respectively, on a volcano plot comparing *P* value versus fold-change for probes from double transductants (*Foxp3* and *Pparg1*, **c**; *Foxp3* and *Pparg2*, **d**) versus single transductants (*Foxp3* alone). The VAT T<sub>reg</sub> cell up- and down-signatures were defined in Methods. *P* values from a chi-squared test. **d**, **e**, Twenty-four hours after transduction of naive CD4<sup>+</sup> T cells, cultures were treated with Pio (1  $\mu$ M) for 48 h. FC/FC plots comparing gene expression values of Pio-treated versus vehicle-treated double transductants (*Pparg1* plus *Foxp3*, **d**; *Pparg2* plus *Foxp3*, **e**) (*x*-axis), and equivalent Pio-treated versus vehicle-treated single transductants (*Foxp3* alone) (*y*-axis). Some genes involved in lipid metabolism are indicated. Mean expression values calculated from three independent experiments. **f**, The association of Foxp3 with PPAR- $\gamma$  was determined by co-immunoprecipitation. An anti-PPAR- $\gamma$ 1+2 antibody was used to immunoprecipitate (IP) PPAR- $\gamma$ 1 and PPAR- $\gamma$ 2 from nuclear lysates of HEK293 cells co-transduced with *Foxp3* and *Pparg1* or *Pparg2*. Immunoblots were probed with anti-Foxp3.

representation of T<sub>reg</sub> cells in the lymphoid organs of mutants was normal (Fig. 3a). Although VAT T<sub>reg</sub> cells in wild-type mice increased >2.5-fold between 15 and 25 weeks to eventually constitute more than 40% of the CD4<sup>+</sup> T cell compartment, this subset remained below ~10% in the mutant mice (Supplementary Fig. 3a). The T<sub>reg</sub> cells remaining in the VAT (but not those in the spleen) of mutants had a lower mean fluorescence intensity (MFI) of *Foxp3* expression than that of their wild-type counterparts (Supplementary Fig. 3b). A volcano plot comparing gene expression in VAT T<sub>reg</sub> cells from *Pparg* wild-type and mutant mice showed the VAT T<sub>reg</sub> cell up-signature (pink, skewed to the right) to be underrepresented in mutant T cells, whereas, conversely, the down-signature (green, skewed to the left) was overrepresented (Fig. 3b). VAT and lymphoid organ T<sub>reg</sub> cells were much more similar in the *Pparg* mutant than in the wild-type mice (Supplementary Fig. 3c); this difference reflected alterations at the level

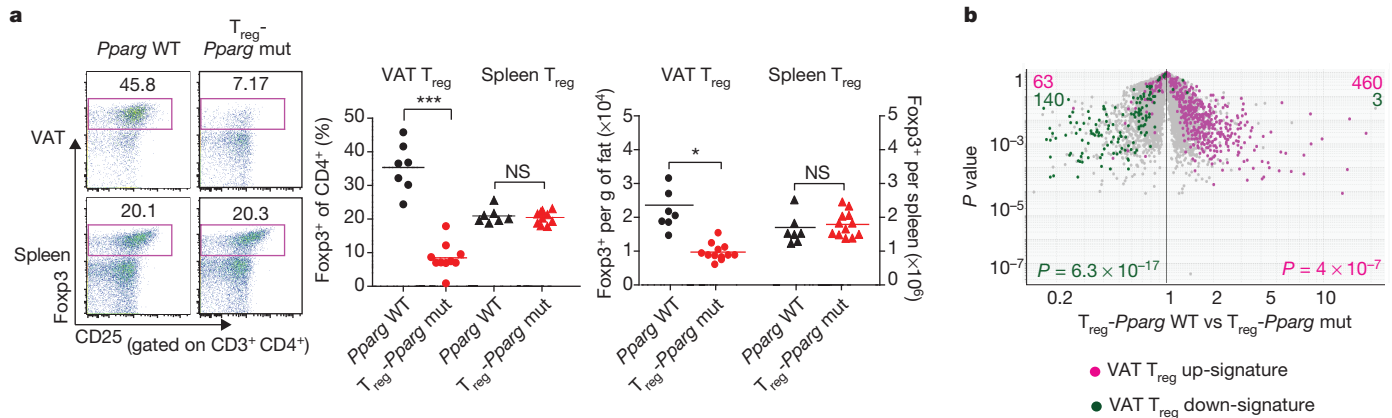


**Figure 3** | *In vivo* effects of abrogating PPAR- $\gamma$  expression specifically in T<sub>reg</sub> cells. **a**, T<sub>reg</sub> cell representation. Cells were isolated from the spleen or stromovascular fraction (SVF) of epididymal fat (epi-fat) of 25-week-old mice lacking PPAR- $\gamma$  specifically in T<sub>reg</sub> cells (T<sub>reg</sub>-*Pparg* mut) or littermate controls. T<sub>reg</sub> cells are defined as CD45<sup>+</sup> CD3<sup>+</sup> CD4<sup>+</sup> Foxp3<sup>+</sup>. Left, representative dot plots (of at least three experiments); centre, summary data (for fraction of CD4<sup>+</sup> cells); right, cell numbers per g of tissue. Dot plot numbers indicate the

percentage of cells in that gate for that particular experiment. \* $P < 0.05$ ; \*\*\* $P < 0.001$  (Student's *t*-test); NS, not significant; WT, wild type. The mean values are shown. **b**, Expression of VAT T<sub>reg</sub> cell signature genes in mutant mice (T<sub>reg</sub>-*Pparg* mut). A volcano plot comparing *P* value versus fold-change for probes from wild-type versus mutant VAT T<sub>reg</sub> cells. Genes from the VAT T<sub>reg</sub> up- and down-signature are highlighted in pink and green, respectively. *P* values from a chi-squared test.

of VAT T<sub>reg</sub> cells, as the absence of PPAR- $\gamma$  expression in lymph node T<sub>reg</sub> cells had little impact (Supplementary Fig. 3d). This observation was confirmed at the protein level (Supplementary Fig. 4): downregulation of CCR2, GATA3, KLRG1 and CD69 in mutant versus wild-type VAT T<sub>reg</sub> cells to resemble the lower levels in lymphoid tissue T<sub>reg</sub> cells; upregulation of CD103 and CD86 in mutant VAT T<sub>reg</sub> cells to approach the higher levels in lymphoid T<sub>reg</sub> cells. Thus, PPAR- $\gamma$  is an important factor controlling the accumulation and phenotype of T<sub>reg</sub> cells residing in adipose tissue.

How the loss of PPAR- $\gamma$  influences the turnover of T<sub>reg</sub> cells residing in VAT is unclear. Addressing this issue was more complex than simply comparing the half-life of VAT T<sub>reg</sub> cells in wild-type and mutant mice because the residual T<sub>reg</sub> cells in the latter animals are likely to be atypical 'survivors' and/or recruits from the lymphoid T<sub>reg</sub> cell pool exploiting a niche empty of the usual competitors. So we performed an acute assay, monitoring T<sub>reg</sub> cell populations in wild-type mice over a few days of treatment with the irreversible PPAR- $\gamma$  inhibitor GW9662 (Supplementary Fig. 5a). There were no significant differences in the VAT or spleen T<sub>reg</sub> cell fraction or numbers in the drug- versus vehicle-treated animals (Supplementary Fig. 5b, c). However, there was a progressive decline in the fraction of GATA3<sup>+</sup> T<sub>reg</sub> cells in VAT (but not in spleen), and a parallel decrease in the GATA3 MFI (Supplementary Fig. 5d, e). The GATA3 transcription factor is highly overrepresented in VAT versus lymphoid tissue T<sub>reg</sub> cells, and is downregulated in the absence of PPAR- $\gamma$  (Supplementary Fig. 4). Altogether, our data indicate that PPAR- $\gamma$  may control both the establishment and the maintenance of the VAT T<sub>reg</sub> cell phenotype.

Secondarily, the mutant mice had fractional and numerical increases in some, but not all, adipose tissue monocyte/macrophage subsets: pro-inflammatory CD11b<sup>+</sup> CD11c<sup>+</sup> F4/80<sup>+</sup> macrophages (Supplementary Fig. 6a, c) and pro-inflammatory CD11b<sup>+</sup> Ly6c<sup>hi</sup> monocytes (left panels in Supplementary Fig. 6b, d), but not CD11b<sup>+</sup> Ly6c<sup>low</sup> monocytes (right panels in Supplementary Fig. 6b, d), considered to be anti-inflammatory. There were no changes in the fractions or numbers of CD8<sup>+</sup> T or B cells in VAT of mutant mice (Supplementary Fig. 6e-h).

Pio is a well-known insulin-sensitizing agent that improves metabolic indices in obese mice and humans. Given its ability to enhance the unique fat T<sub>reg</sub> cell signature in cultured cells (Fig. 2d, e), we wondered how this drug might affect VAT T<sub>reg</sub> cells in obese (HFD-fed) mice. There was an impressive enrichment of the fraction and number of T<sub>reg</sub> cells in epididymal adipose tissue of animals treated with Pio (Fig. 4a and Supplementary Fig. 7a); this effect was specific,

and not seen in the spleen, subcutaneous fat, perirenal fat or liver (Fig. 4a and Supplementary Fig. 7b). There were also marked phenotypic changes in the epididymal fat T<sub>reg</sub> cell population of Pio-treated and equivalent untreated obese mice: an overall shift of the gene expression profile towards that typical of VAT T<sub>reg</sub> cells (Fig. 4b); an increase in the Foxp3 MFI (Supplementary Fig. 7c); a PPAR- $\gamma$ -dependent enrichment of cells expressing GATA3 (Supplementary Fig. 7d); and enhanced cell-surface display of the lipid scavenger CD36 (Fig. 4c). As PPAR- $\gamma$  ligands are known to stimulate oxidized low-density lipoprotein uptake by augmenting levels of CD36 on the surface of macrophages<sup>6</sup>, we stained T<sub>reg</sub> cells with Nile red, a dye that selectively binds to intracellular lipid droplets. VAT, but not spleen, T<sub>reg</sub> cells readily took up lipids, especially in response to Pio (Fig. 4d). This process was PPAR- $\gamma$ -dependent as the Pio-induced increase in CD36 expression and Nile red staining were both greatly dampened in *Pparg* mutant mice (Supplementary Fig. 7e, f). Thus, Pio accentuates the accumulation and phenotype of fat T<sub>reg</sub> cells in epididymal fat depots of obese mice.

The marked increase in the representation of and alterations in the phenotype of VAT T<sub>reg</sub> cells provoked by Pio treatment of obese mice raised the question of whether this population contributes to the insulin-sensitizing effect of Pio. In analogy to the human context, we compared immunological and metabolic parameters in obese (HFD-fed) *Pparg* wild-type and mutant mice as a function of Pio co-treatment. As anticipated, the VAT T<sub>reg</sub> cell population of wild-type animals fed a HFD was quite low, and it increased substantially when Pio was included in the diet (Fig. 4e). Also as expected, the representation of VAT T<sub>reg</sub> cells in mutant animals on a HFD was similar to that of their wild-type counterparts: a HFD in and of itself results in death and/or evacuation of typical VAT T<sub>reg</sub> cells, so abrogation of PPAR- $\gamma$  expression in this context has no further effect. Pio could not expand VAT T<sub>reg</sub> cells in the mutant (Fig. 4e). Pio had differential effects on conventional adipose tissue monocyte/macrophage populations in HFD-fed mutant mice: pro-inflammatory macrophages (CD11b<sup>+</sup> CD11c<sup>+</sup> F4/80<sup>+</sup>) were diminished, although not to the degree seen in wild-type littermates (Supplementary Fig. 8a); by contrast, pro-inflammatory monocytes (CD11b<sup>+</sup> Ly6c<sup>hi</sup>) did not undergo their usual reduction (Supplementary Fig. 8b, left); whereas anti-inflammatory monocytes (CD11b<sup>+</sup> Ly6c<sup>low</sup>) uncharacteristically declined (Supplementary Fig. 8b, right). Pio treatment of obese mutant mice was less effective than the treatment of their wild-type counterparts at normalizing systemic metabolic parameters: homeostatic model assessment of insulin resistance (Fig. 4f), glucose and insulin tolerance

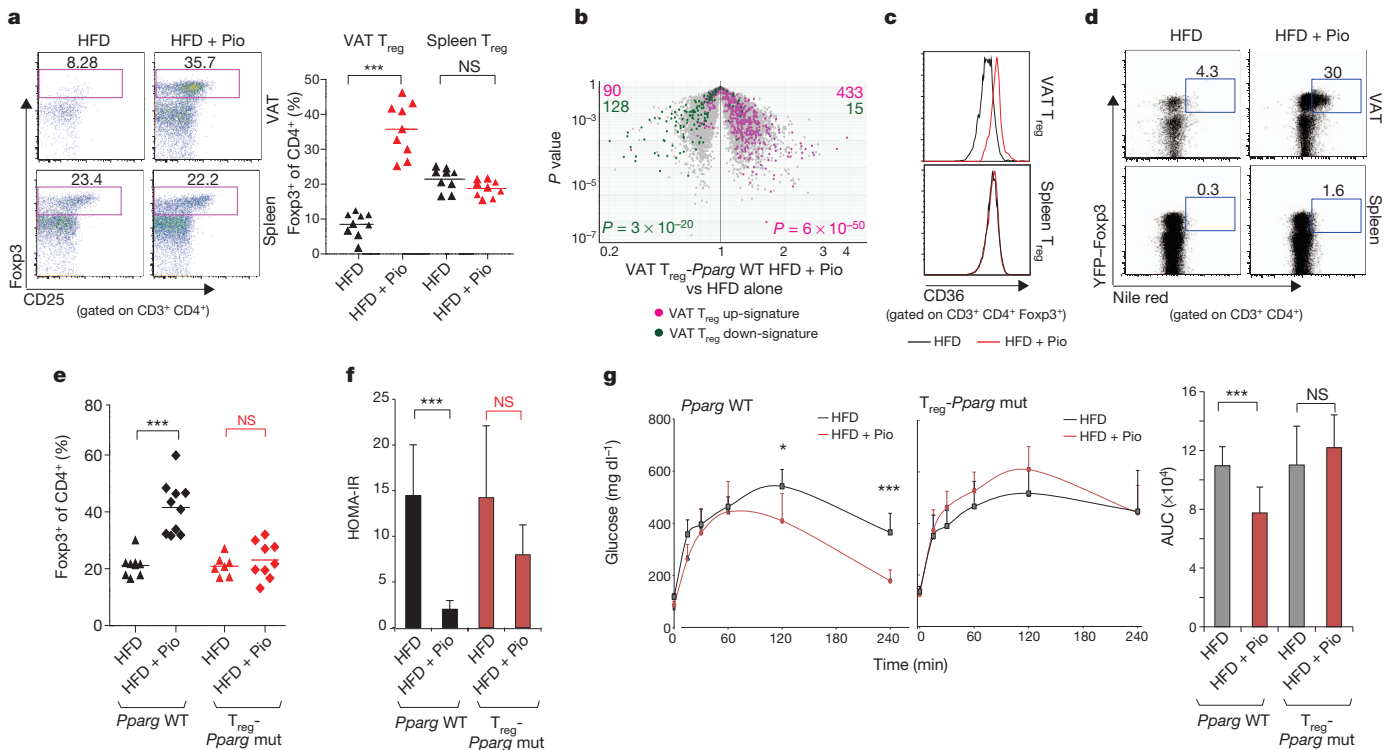


**Figure 4 | Pio promotion of epididymal fat T<sub>reg</sub> cell numbers and phenotype.** At 9 weeks of age, wild-type and mutant *Pparg* mice ( $T_{reg}^{-/-}$  *Pparg* mut) were fed a HFD with or without Pio for 13 weeks. Cells from the spleen and epididymal fat SVF were stained and analysed by flow cytometry. Numbers on dot plots indicate the percentage of cells in that gate for that particular experiment (representative of at least three experiments). **a**, T<sub>reg</sub> cells from *Pparg* wild-type mice on a HFD with or without Pio. Left, representative dot plots; right, summary data. **b**, Expression of VAT T<sub>reg</sub> cell signature genes in *Pparg* wild-type mice on a HFD with or without Pio. Volcano plot compares *P* value versus fold-change for probes from VAT T<sub>reg</sub> cells isolated from *Pparg* wild-type mice on a HFD plus Pio versus a HFD alone. Genes from the VAT T<sub>reg</sub> up- and down-signature are highlighted in pink and green, respectively. *P* values from a chi-squared test. **c**, MFI of CD36 expression by T<sub>reg</sub> cells. ΔMFI indicates, for gated CD3<sup>+</sup> CD4<sup>+</sup> Foxp3<sup>+</sup> cells, the difference in CD36

(Fig. 4g and Supplementary Fig. 8c), and phosphorylated (p)AKT levels in multiple organs (Supplementary Fig. 8d). At least some of the muted metabolic response to Pio reflected events in VAT, evidenced by the lack of normalization of pAKT values at that site. The Pio treatment clearly worked, however, as we observed in both wild-type and mutant drug-treated HFD-fed mice the expected increase in epididymal fat-pad weight (Supplementary Fig. 9a), although not in total body weight (not shown); a coupled decrease in adipocyte numbers and an increase in adipocyte size (Supplementary Fig. 9b, c); and increased levels of serum adiponectin and *Adipoq* transcripts (Supplementary Fig. 9d). Leptin (*Lep*) transcript levels were unchanged in both wild-type and HFD-fed individuals (Supplementary Fig. 9e), as anticipated<sup>7</sup>.

The main conclusion from our results is that PPAR- $\gamma$  is a major orchestrator of the unique properties of VAT T<sub>reg</sub> cells. This nuclear receptor collaborates with Foxp3 to impose on naive CD4<sup>+</sup> T cells the transcriptional profile characteristic of VAT T<sub>reg</sub> cells. Interestingly, both PPAR- $\gamma$  isoforms can promote the fat T<sub>reg</sub> up-signature in conjunction with Foxp3, but only isoform 1 drives the down-signature. This constitutes a rare dysjunction in the activities of the two PPAR- $\gamma$  isoforms, which differ by only an extra 30 amino acids at the amino terminus of PPAR- $\gamma$ 2. Experimental manipulation of PPAR- $\gamma$  specifically in Foxp3<sup>+</sup> cells had a clear and precise impact on the accumulation and phenotype of T<sub>reg</sub> cells in epididymal fat depots. A newly discovered property was that VAT, but not lymphoid tissue, T<sub>reg</sub> cells

expression for HFD-fed mice with or without Pio treatment. Epi-fat ΔMFI =  $3,828 \pm 1,362$  ( $*P = 0.039$ ); spleen ΔMFI =  $-182 \pm 597$  (NS). **d**, Cells were isolated from the spleen or epi-fat SVF of B6. *Foxp3*-(YFP)-*Cre* mice kept on a HFD with or without Pio for 13 weeks, and stained for CD3, CD4 and Nile red. YFP, yellow fluorescent protein.  $*P = 0.01$ . **e**, T<sub>reg</sub> cell fraction. Cells from spleen or epi-fat SVF were stained and analysed by flow cytometry. **f**, Insulin sensitivity. Mice were assessed for blood fasting-glucose and fasting-insulin levels. These values were used to calculate the homeostatic model assessment of insulin resistance (HOMA-IR). **g**, Glucose tolerance test. Left, intraperitoneal glucose tolerance test (GTT) on wild-type mice. Centre, GTT on mutant mice. Right, area under the curve (AUC) calculations.  $n = 13$ –14 mice per group.  $*P < 0.05$ ,  $***P < 0.001$  (Student's *t*-test). Error bars denote mean  $\pm$  s.d. for immunological parameters, mean  $\pm$  s.e.m. for metabolic parameters, as is standard practice in the respective fields.

can take up lipids, an intriguing adaptation to the tissular environment, not shared by conventional T cells residing at the same site. It remains to be determined whether this feature promotes T<sub>reg</sub> cell survival or effector functions, or whether it is an epiphenomenon.

Our data also indicate that PPAR- $\gamma$  expressed by T<sub>reg</sub> cells contributes substantially to the insulin-sensitizing activity of Pio. It was initially assumed, given the role of this transcription factor in fat-cell differentiation, that TZD drugs improve metabolic parameters in obese individuals by activating PPAR- $\gamma$  in adipocytes. Although this notion has received experimental support<sup>8</sup>, other studies have argued for the importance of PPAR- $\gamma$  expression in macrophages<sup>9,10</sup>, muscle<sup>11</sup> and the central nervous system<sup>12,13</sup>. On first consideration, it seems difficult to explain the need for PPAR- $\gamma$  across such a broad range of cell types, but several points should be kept in mind. First, TZD drugs may affect several processes upstream of insulin resistance, for example, ingestive behaviour, adiposity and inflammation; PPAR- $\gamma$ -driven programs in different cell types may influence these processes differentially. Second, abrogating PPAR- $\gamma$  expression in different cell types seems to have organ-specific effects on insulin resistance<sup>11–13</sup>. And third, there is increasing appreciation that the gene promoters used to generate transgenic mouse lines with cell-type-specific ablation of PPAR- $\gamma$  can be 'leaky'. Delineating the cell type(s) crucial for the protective effect of Pio on metabolic disorders is imperative given current concerns over the side effects of the TZD class of compounds and the resultant search for alternative drugs<sup>14</sup>.

Lastly, our results provide proof-of-principle that it is possible to target a designated population of T<sub>reg</sub> cells for a particular therapeutic goal. The emerging notion that the Foxp3<sup>+</sup> CD4<sup>+</sup> T<sub>reg</sub> cell compartment includes several subtypes with distinct phenotypes, localizations and effector functions<sup>15</sup> has evoked the exciting possibility of developing strategies to expand or contract disease-relevant T<sub>reg</sub> cells, leaving the bulk of the compartment intact to maintain immune homeostasis.

## METHODS SUMMARY

Source and maintenance of mice are described in Methods. Experimentals and controls were always littermate-matched males (for example, *Pparg*<sup>fl/fl</sup>-*Foxp3*<sup>YFP-Cre</sup> and *Pparg*<sup>wt</sup>-*Foxp3*<sup>YFP-Cre</sup>). HFD and normal-chow animals were fed a diet containing 60 kcal% and 10 kcal% fat, respectively. Mice on a HFD plus Pio were fed Pio at 100 mg per kg of food. Metabolic studies were performed on mice fed a HFD with or without Pio for 12 weeks. For GTTs, glucose (2.0 g per kg body weight) was administered by intraperitoneal (i.p.) injection after an overnight fast. For insulin tolerance tests, insulin (0.75 U) was administered by i.p. injection after 4 h of fasting.

CD4<sup>+</sup> CD25<sup>-</sup> T cells were activated for 48 h with anti-CD3/CD28 antibody-coated beads plus recombinant human IL-2 before retroviral transduction and cultured for 72 h after transduction. In selected experiments, 24 h after infection, transduced cells were treated with 1 μM Pio, rosiglitazone or GW1929, or with vehicle (dimethylsulphoxide) for 48 h before sorting. For T-cell analysis, cells were stained with anti-CD45, -CD3, -CD4, -CD8, -CD25 and sometimes anti-CD36, fixed, permeabilized and intracellularly stained for Foxp3 and GATA3. For intracellular lipids, cells were stained with anti-CD3, anti-CD4 and Nile red (1 μg ml<sup>-1</sup>). RNA from double-sorted cells was prepared for microarray analysis<sup>2</sup>, and hybridized to GeneChip Mouse Genome M1.0 ST arrays (Affymetrix).

**Full Methods** and any associated references are available in the online version of the paper at [www.nature.com/nature](http://www.nature.com/nature).

**Received 21 June 2011; accepted 3 April 2012.**

**Published online 16 May 2012.**

- Osborn, O. & Olefsky, J. M. The cellular and signaling networks linking the immune system and metabolism in disease. *Nature Med.* **18**, 363–374 (2012).
- Feuerer, M. *et al.* Lean, but not obese, fat is enriched for a unique population of regulatory T cells that affect metabolic parameters. *Nature Med.* **15**, 930–939 (2009).
- Winer, S. *et al.* Normalization of obesity-associated insulin resistance through immunotherapy. *Nature Med.* **15**, 921–929 (2009).

- Ilan, Y. *et al.* Induction of regulatory T cells decreases adipose inflammation and alleviates insulin resistance in ob/ob mice. *Proc. Natl Acad. Sci. USA* **107**, 9765–9770 (2010).
- Tontonoz, P. & Spiegelman, B. M. Fat and beyond: the diverse biology of PPARγ. *Annu. Rev. Biochem.* **77**, 289–312 (2008).
- Tontonoz, P. *et al.* PPARγ promotes monocyte/macrophage differentiation and uptake of oxidized LDL. *Cell* **93**, 241–252 (1998).
- Miyazaki, Y. *et al.* Effect of pioglitazone on circulating adipocytokine levels and insulin sensitivity in type 2 diabetic patients. *J. Clin. Endocrinol. Metab.* **89**, 4312–4319 (2004).
- Sugii, S. *et al.* PPARγ activation in adipocytes is sufficient for systemic insulin sensitization. *Proc. Natl Acad. Sci. USA* **106**, 22504–22509 (2009).
- Hevener, A. L. *et al.* Macrophage PPARγ is required for normal skeletal muscle and hepatic insulin sensitivity and full antidiabetic effects of thiazolidinediones. *J. Clin. Invest.* **117**, 1658–1669 (2007).
- Odegaard, J. I. *et al.* Macrophage-specific PPARγ controls alternative activation and improves insulin resistance. *Nature* **447**, 1116–1120 (2007).
- Hevener, A. L. *et al.* Muscle-specific *Pparg* deletion causes insulin resistance. *Nature Med.* **9**, 1491–1497 (2003).
- Ryan, K. K. *et al.* A role for central nervous system PPAR-γ in the regulation of energy balance. *Nature Med.* **17**, 623–626 (2011).
- Lu, M. *et al.* Brain PPAR-γ promotes obesity and is required for the insulin-sensitizing effect of thiazolidinediones. *Nature Med.* **17**, 618–622 (2011).
- Olefsky, J. M., Lazar, M. A. & Scherer, P. E. Antidiabetes wars: a new hope. *Nature Med.* **16**, 972–973 (2010).
- Josefowicz, S. Z., Lu, L. F. & Rudensky, A. Y. Regulatory T cells: mechanisms of differentiation and function. *Annu. Rev. Immunol.* **30**, 531–563 (2012).

**Supplementary Information** is linked to the online version of the paper at [www.nature.com/nature](http://www.nature.com/nature).

**Acknowledgements** We thank A. Rudensky, F. Gonzalez, R. Kahn, B. Spiegelman and D. Vignali for providing materials; K. Hattori, M. Davenport, J. LaVecchio, G. Buruzala, J. Ericson, K. Leatherbee and S. Davis for technical assistance; A. Ergun, A. Morton and J. Shu for experimental help; and M. Wilson and J. Hill for discussions. Supported by grants from the National Institutes of Health (NIH; DK092541) and Ellison Foundation (Boston) to D.M. and C.B., Dana Foundation to D.M. and S.E.S.; the American Diabetes Association (RA 110BS97) to J.L., and the NIH (DK51729) to S.E.S.; as well as by core facilities of the Joslin Diabetes Center (P30DK36836). M.F. received a postdoctoral fellowship from the King Trust.

**Author Contributions** All authors designed research; D.C. and A.L. performed research; D.C., S.E.S., C.B. and D.M. analysed data; D.C., C.B. and D.M. wrote the paper.

**Author Information** Microarray data have been deposited in the Gene Expression Omnibus under accession codes GSE37532, GSE37533, GSE37534 and GSE37535. Reprints and permissions information is available at [www.nature.com/reprints](http://www.nature.com/reprints). The authors declare competing financial interests: details accompany the full-text HTML version of the paper at [www.nature.com/nature](http://www.nature.com/nature). Readers are welcome to comment on the online version of this article at [www.nature.com/nature](http://www.nature.com/nature). Correspondence and requests for materials should be addressed to D.M. ([cbdm@hms.harvard.edu](mailto:cbdm@hms.harvard.edu)).

## METHODS

**Mice.** Male B6, B6.*Lep<sup>ob/ob</sup>*, B6.*Foxp3<sup>YFP-Cre</sup>* (ref. 16) and B6.*Pparg*-floxed (ref. 17) mice were bred in our specific pathogen-free facilities at Harvard Medical School or the Joslin Diabetes Center, or were purchased from the Jackson Laboratory. Mutant *Pparg* T<sub>reg</sub> cell mice (T<sub>reg</sub>-*Pparg* mut) were generated by crossing B6.*Foxp3<sup>YFP-Cre</sup>* and B6.*Pparg*-floxed mice. HFD animals were fed a diet of 60 kcal% fat from Research Diets. Normal chow control animals were fed a diet containing 10 kcal% fat from the same vendor. Mice on a HFD plus Pio were fed Pio (Actos, Takeda) at 100 mg per kg of food. Experimentals and controls were always littermate-matched males (*Pparg<sup>fl/fl</sup>*-*Foxp3<sup>YFP-Cre</sup>* and *Pparg<sup>wt</sup>*-*Foxp3<sup>YFP-Cre</sup>*).

**Metabolic studies.** In designated experiments, mice were fed a HFD with or without Pio from 9 to 22 weeks of age. Metabolic studies were performed at 4, 8 and 12 weeks of feeding; at each time point, mice were fasted for 14 h overnight, weighed and then tested for fasting blood glucose and insulin concentrations (by ELISA). At the last time point (12–13 weeks of feeding), we also measured serum adiponectin (by ELISA) and performed GTTs, insulin tolerance tests (ITTs) and insulin signalling pathway analysis. For GTTs, glucose (2.0 g per kg body weight) was administered by intraperitoneal (i.p.) injection after an overnight fast. Blood glucose levels were measured before and 15, 30, 60, 120 and 240 min after glucose injection. For ITTs, insulin (0.75 U, Humulin R, Lilly) was administered by i.p. injection after 4 h of fasting. Blood glucose levels were measured before and 20, 40, 60, 80, 100 and 120 min after insulin injection. For insulin signalling pathway analysis, overnight-fasted mice were anaesthetized, injected through the inferior vena cava with 5 U insulin (Humulin R, Lilly) or PBS, and were euthanized after 5 min. Collected epi-fat, liver and muscle were stored until use in liquid N<sub>2</sub>, homogenized with a Polytron for 30 s in lysis buffer (30 mM HEPES, 150 mM NaCl, 1 mM phenylmethylsulfonyl fluoride, 3 μM aprotinin, 10 μM leupeptin, 5 μM pepstatin A, 25 mM benzamide, 25 mM sodium vanadate, 5 mM glycerol phosphate, 100 mM NaF, 1.0 mM ammonium molybdate, 30 mM tetrasodium pyrophosphate, 5 mM EGTA, 10% glycerol, 1% Triton X-100 and 0.5% sodium deoxycholate, pH 7.4). Total tissue protein was assayed by western blotting for pAKT (anti-Ser 473, Cell Signaling) and AKT (Cell Signaling). All ELISA measurements were performed by the Joslin Diabetes Center's Specialized Assay Core.

**Isolation of T and myeloid cells.** Epididymal, subcutaneous or perirenal adipose tissue, and liver were excised after flushing the organs through the portal vein and the heart ventricle, cut into small pieces (or passed through a sieve in the case of the liver), and digested for 20 min with collagenase type II (Sigma). Cell suspensions were then filtered through a sieve, and the SVF fraction was collected after centrifugation at 450g for 10 min. For T-cell analysis, cells were stained with anti-CD45 (clone 30-F11), -CD3 (145-2C11), -CD4 (GK1.5), -CD8 (5H10) and -CD25 (PC61) antibodies (from BioLegend) (and with anti-CD36 for some experiments); and were fixed, permeabilized and intracellularly stained for Foxp3 (FJK-16s) and GATA3 (TWAJ) according to the manufacturer's instructions (eBiosciences). For myeloid cell analysis, cells were stained with anti-CD45, -TCR-β (H57–597), -CD11b (M1/70), -CD11c (N418), F4/80 (CI.A3-1), and anti-Ly6c (HK1.4) from BioLegend. B cells were stained with anti-CD45, -CD3 and -CD19 (6D5). For intracellular lipids, cells were stained with anti-CD3, -CD4 and Nile red (Enzo Life Sciences) (1 μg ml<sup>-1</sup>). Cells were double-sorted using the MoFlo, or analysed using an LSRII instrument (BD Bioscience) and FlowJo software.

**Histology.** Epi-fat was excised and fixed in 10% buffered formalin. Sectioning and haematoxylin/eosin staining were performed by the Joslin Diabetes Center's Histology Core.

**Retroviral transduction of CD4<sup>+</sup> T cells.** Cells were collected from spleens and lymph nodes of 6–8-week-old B6 mice. After mechanical dissociation and red blood cell lysis, remaining cells were labelled with phycoerythrin-conjugated anti-CD11b, -CD11c, -B220 (RA3-6B2), -CD19 (6D5), -CD8, -CD25 and -NK1.1 (PK136), and were selected by MACS column purification. The negative fraction was collected and tested for purity by flow cytometry (~97%). CD4<sup>+</sup> CD25<sup>-</sup> T cells were then activated with anti-CD3/CD28 antibody-coated beads (Invitrogen) at concentrations of one bead per cell in the presence of 20 U ml<sup>-1</sup> recombinant human IL-2 (Proleukin; Chiron). T cells were cultured for 48 h before retroviral transduction. Viruses were prepared by transfecting platE cells<sup>18</sup> with retroviral expression plasmids (MSCV IRES-GFP (pMIG2) and IRES-Thy1.1 (pMIT2))<sup>19</sup>, encoding *Foxp3* (GFP), *Pparg1* (Thy1.1) or *Pparg2* (Thy1.1), and the packaging construct pCL-ECO<sup>20</sup> using TransIT-293 (Mirus), according to the manufacturer's

instructions. Naive CD4<sup>+</sup> T cells were infected with retroviral supernatants at 48 h, and were subsequently cultured for a further 72 h. Singly (*Foxp3*) or doubly (*Foxp3* plus *Pparg1* or *Pparg2*) transduced cells were double-sorted as (CD11b<sup>-</sup> CD11c<sup>-</sup> B220<sup>-</sup> CD8<sup>-</sup>) CD3<sup>+</sup> CD4<sup>+</sup> GFP<sup>+</sup> (and/or Thy1.1<sup>+</sup>) by MoFlo for RNA processing and microarray analysis. In selected experiments, 24 h after cell infection, single and double transductants were treated with 1 μM Pio (Enzo Life Sciences), rosiglitazone (Enzo Life Sciences) or GW1929 (Enzo Life Sciences)<sup>21</sup>, or with vehicle (dimethylsulphoxide) for 48 h before sorting. pMIT2 vector was generated by swapping the GFP reporter gene of pMIG2 with Thy1.1. *Pparg1* and *Pparg2* complementary DNAs were purchased from Addgene (plasmid 8886 and 8862, respectively) and were cloned into the pMIT2 vector.

**Microarray analysis.** Lymph node and VAT CD3<sup>+</sup> CD4<sup>+</sup> CD25<sup>hi</sup> (T<sub>reg</sub> cells) or CD3<sup>+</sup> CD4<sup>+</sup> CD25<sup>-</sup> (conventional T cells (T<sub>conv</sub>)) cells were double-sorted from B6, B6.*Lep<sup>ob/ob</sup>*, *Pparg* wild-type and mutant mice. From the retroviral transduction experiment, CD3<sup>+</sup> CD4<sup>+</sup> GFP<sup>+</sup> (that is, Foxp3<sup>+</sup>) single-transduced cells or CD3<sup>+</sup> CD4<sup>+</sup> GFP<sup>+</sup> Thy1.1<sup>+</sup> (that is, expressing Foxp3 and PPAR-γ1 or PPAR-γ2) double-transduced cells, treated with Pio or vehicle, were double-sorted. RNA was extracted with trizol and amplified for two rounds using the MessageAmp aRNA kit (Ambion), followed by biotin labelling using the BioArray High Yield RNA Transcription Labeling Kit (Enzo Diagnostics), and was purified using the RNeasy Mini Kit (Qiagen). The resulting complementary RNAs (three independent datasets for each sample type) were hybridized to GeneChip Mouse Genome M1.0 ST chip arrays (Affymetrix) according to the manufacturer's protocol. Initial reads were processed through Affymetrix software to obtain raw .cel files. Microarray data were background-corrected and normalized using the robust multi-array average (RMA) algorithm implemented in the GenePattern software package<sup>22</sup>, and replicates were averaged. The VAT T<sub>reg</sub> cell-specific gene set included loci specifically over- or underexpressed in epi-fat T<sub>reg</sub> cells, and was generated by including genes that were over- or underexpressed by twofold or more in VAT T<sub>reg</sub> cells versus VAT T<sub>conv</sub> cells, lymph node T<sub>conv</sub> and lymph node T<sub>reg</sub> cells. *k*-means clustering was performed on the T<sub>reg</sub> cell profiles from VAT and lymph nodes of B6 mice (on normal chow or HFD) or B6.*Lep<sup>ob/ob</sup>* mice of different ages to identify the *Pparg* co-cluster and anti-cluster. Interpretation of results as well as our extensive library of diverse T cells microarray datasets benefited from data assembled by the ImmGen consortium (<http://www.immgen.org>)<sup>23</sup> (details available on request).

**Quantitative PCR analysis.** Epi-fat tissue was frozen in liquid N<sub>2</sub> and homogenized in trizol before RNA extraction (RNeasy Lipid Tissue Mini Kit). RNA was reverse transcribed with oligo(dT) primers and SuperScript Polymerase 2 (Invitrogen). Real-time quantitative PCR was performed using gene-specific fluorogenic assays (TaqMan; Applied Biosystems). Transcript levels were normalized to those from the mouse *Hprt* gene.

**Co-immunoprecipitation experiments.** Nuclear extracts from transfected HEK293 cells transduced with *Foxp3* and with *Pparg1* or *Pparg2* were prepared in nuclear lysis buffer (Active Motif) according to the manufacturer's protocol. Immunoprecipitation was carried out using anti-PPAR-γ1+2-coated Protein G-Sepharose beads (GE Healthcare) followed by western blotting with anti-Foxp3 (FJK-16s, eBioscience) and anti-PPAR-γ1+2 (A3409A, Abcam).

- Rubtsov, Y. P. *et al.* Regulatory T cell-derived interleukin-10 limits inflammation at environmental interfaces. *Immunity* **28**, 546–558 (2008).
- Akiyama, T. E. *et al.* Conditional disruption of the peroxisome proliferator-activated receptor γ gene in mice results in lowered expression of ABCA1, ABCG1, and apoE in macrophages and reduced cholesterol efflux. *Mol. Cell Biol.* **22**, 2607–2619 (2002).
- Morita, S., Kojima, T. & Kitamura, T. Plat-E: an efficient and stable system for transient packaging of retroviruses. *Gene Ther.* **7**, 1063–1066 (2000).
- Holst, J. *et al.* Generation of T-cell receptor retrogenic mice. *Nature Protoc.* **1**, 406–417 (2006).
- Naviaux, R. K., Costanzi, E., Haas, M. & Verma, I. M. The pCL vector system: rapid production of helper-free, high-titer, recombinant retroviruses. *J. Virol.* **70**, 5701–5705 (1996).
- Leesnitzer, L. M. *et al.* Functional consequences of cysteine modification in the ligand binding sites of peroxisome proliferator activated receptors by GW9662. *Biochemistry* **41**, 6640–6650 (2002).
- Reich, M. *et al.* GenePattern 2.0. *Nature Genet.* **38**, 500–501 (2006).
- Heng, T. S. & Painter, M. W. The Immunological Genome Project: networks of gene expression in immune cells. *Nature Immunol.* **9**, 1091–1094 (2008).